Environmental Science and Pollution Research
https://doi.org/10.1007/s11356-020-08819-9

RESEARCH ARTICLE

Conversion synthesis of manganese sulfate residue into iron hydroxide adsorbent for Cu(II) removal from aqueous solution

Shicheng Ma[1] · Hannian Gu[2] · Zaimei Mei[1] · Yongqiong Yang[1] · Ning Wang[2]

Received: 9 December 2019 / Accepted: 7 April 2020

Abstract

Manganese sulfate residue (MSR) is a by-product derived from the manganese sulfate production process. In this study, an iron hydroxide adsorbent was prepared from MSR using the hydrothermal conversion method. The adsorbent was characterized and used to remove copper(II) ions from aqueous solution. Batch experiments were performed to investigate the adsorption efficiency of copper ions at different contact times, initial concentrations, solution pH levels, and reaction temperatures. Adsorption equilibrium was observed in 3 h, and the best pH was under natural conditions (pH ~ 5.5). Increasing the initial Cu^{2+} concentration and reaction temperature can increase the adsorption quantity. The adsorption capacity of iron hydroxide at an initial concentration of 50 mg L^{-1} was 14.515 mg g^{-1} Cu(II) under the conditions of a nature pH and room temperature. According to the adsorption data, the pseudo-second-order model can describe the adsorption kinetics of copper ions well, and the Freundlich model provides an excellent fit to the adsorption isotherm. XRD and FTIR were applied to characterize the raw materials and adsorbents to reveal the adsorption mechanism. The results suggest that the adsorbent converted from MSR is a promising material for the removal of Cu(II) in aqueous solutions.

Keywords Manganese sulfate residue · Copper ions · Iron hydroxide · Adsorption capacity · Kinetic model

Introduction

Manganese has been widely used and is considered one of the important strategic resources (Lan et al. 2019). Pyrolusite (MnO_2) is one of the most common manganese-bearing minerals in producing manganese sulfate. Manganese sulfate residue (MSR) is discharged as a kind of industrial waste during the sulfuric acid leaching process of manganese-bearing ores (Yang et al. 2018). MSR is different from electrolytic manganese residue (EMR), which usually contains soluble manganese and ammonia nitrogen as contaminants (Shu et al. 2016, 2019a). This occurs because EMR is subjected to a neutralization treatment process using ammonium hydroxide after sulfuric acid leaching. Although MSR and EMR have similar compositions, EMR is more widely reported in the literature (Shu et al. 2019b), because EMR has a high ammonia nitrogen content that could seriously damage the ecological environment and must be separated before utilization (Shu et al. 2016). In addition, the content of iron oxides in MSR is usually higher than that in EMR (Shu et al. 2018; Yang et al. 2018; Lan et al. 2019). MSR samples derived from the leaching process of pyrolusite with different procedures were reported to contain approximately 20 wt% of Fe_2O_3 (Yang et al. 2018). Iron hydroxides can be prepared as adsorbents for metal or anion removal from aqueous solutions (Mezenner and Bensmaili 2009; Wang et al. 2019). Therefore, the higher iron content in MSR can potentially be useful for adsorbent preparation.

Copper has been designated as a heavy metal contaminant, and Cu-containing water can induce serious damage to the environment or even human health (Xie et al. 2017). It has been recognized that the use of low-cost adsorbents to remove

Responsible editor: Tito Roberto Cadaval Jr

Electronic supplementary material The online version of this article (https://doi.org/10.1007/s11356-020-08819-9) contains supplementary material, which is available to authorized users.

✉ Hannian Gu
guhannian@vip.gyig.ac.cn

[1] School of Geography and Environmental Science, Guizhou Normal University, Guiyang 550025, China

[2] Key Laboratory of High-temperature and High-pressure Study of the Earth's Interior, Institute of Geochemistry, Chinese Academy of Sciences, Guiyang 550081, China

Published online: 16 April 2020

metal ions for water decontamination is economically acceptable, especially using the adsorbents prepared from industrial wastes. Numerous adsorbents have been studied for Cu(II) removal, including zeolites from chitosan (Song et al. 2019), graphene (Chen et al. 2018), nanocomposites (Hosseinzadeh et al. 2018), and biocomposites (Garba et al. 2016). However, most of these adsorbents are high cost or require complicated pretreatment processes (Xie et al. 2017). Industrial waste can be used as adsorbents for effectively removing copper ions, such as red mud (Nadaroglu et al. 2010), fly ash (Visa 2016), and agricultural wastes (Pengsaket et al. 2016). Taking advantage of industrial solid waste to prepare adsorbent is a feasible, potential, and promising approach to remove copper ions from wastewater.

The aim of this study was to prepare an iron hydroxide adsorbent via hydrothermal conversion based on MSR as the raw material. The adsorption behavior of the adsorbent for copper ions in aqueous solutions was then studied. The effects of experimental parameters on the adsorption behavior of Cu(II) in aqueous solutions, including balance time, initial Cu(II) concentration, initial solution pH, and experimental temperature, were investigated. In addition, models of the adsorption kinetics and isotherm were assessed based on the experimental data, and relevant parameters with respect to the fitting models were calculated.

Materials and methods

Materials and reagents

The MSR sample used in the current study was obtained from a manganese sulfate production enterprise in Guizhou, China. The fresh MSR sample was firstly crushed, and then dried at 105 °C until a constant weight was achieved. The dried MSR was ground and pulverized into fine powders so as to pass through a 200 mesh sieve. Copper sulfate pentahydrate was purchased from Chengdu Jinshan Chemical Reagent Co. Ltd., China. The hydrochloric acid (HCl, guaranteed reagent) and sulfuric acid (H_2SO_4) used in this study were provided by Sinopharm Group Chemical Reagent Co. Ltd., China. Reagents (expectation for hydrochloric acid) were of analytical grade, and all solutions referred in the experiment were prepared using deionized water.

Adsorbent preparation and characterization

The iron hydroxide adsorbent was prepared via hydrothermal conversion from MSR. Approximately 40 g of ground and sieved MSR was added to a 1000 mL beaker, after which 800 mL of 2 mol L^{-1} HCl was incorporated. The solution was heated and boiled for 1 h. After filtering, the filtrate was diluted to 3200 mL, and aqua ammonia was then used to adjust the pH to 7.0. The precipitate generated during the neutralization process was then separated by filtering. After washing three times with deionized water at 40 °C and then drying at 80 °C for approximately 10 h until a constant weight was attained, converted MSR (CMSR) was obtained as adsorbent, with iron hydroxide as the main composition.

The main chemical components of MSR and CMSR were analyzed by XRF (X-ray fluorescence spectroscopy, PANalytical PW2424, Netherlands). The phase compositions of MSR and CMSR were measured by X-ray diffraction (XRD, PANalytical Empyrean, Netherlands) with Cu Kα radiation. Scanning electron microscopy (SEM, Scios, FEI, USA) was employed to observe the morphology and to qualitatively analyze the element types in the samples. Raman spectrometer (InVia, Renishaw, UK), Fourier transform infrared spectrometer (FTIR, VERTEX 70, Brock, Germany), and X-ray photoelectron spectrometer (XPS, Axis Ultra DLD, Shimadza-Kratos, UK) were used for characterization of adsorbents in this study. The Cu(II) concentrations in the solutions were determined by a flame atomic absorption photometer (AAS, 900F, PE, USA).

Batch adsorption experiments

A certain amount of $CuSO_4 \cdot 5H_2O$ was dissolved in deionized water, and the original solutions with different concentrations (10, 15, 20, 25, 30, and 50 mg L^{-1}) were prepared as stock solutions. Batch adsorption experiments were conducted by adding CMSR adsorbent (0.25 g) and $CuSO_4$ solution (250 mL) into a 500-mL conical flask, and the flask was shaken at an oscillation rate of 200 r min^{-1}. In contrast, the adsorption capacity of the original MSR was determined with Cu^{2+} concentration of 10 mg L^{-1}. The effects of operating parameters for the batch adsorption experiments onto CMSR, such as the contact time, initial Cu(II) concentration, initial pH values and reaction temperature, were also investigated. The solutions pH were adjusted to 2.0–5.0 with 0.05 mol L^{-1} H_2SO_4 solution, and the solutions were analyzed after passing through a 0.45 μm filter membrane. Three sets of parallel experiments were carried out for each sample.

After the experiment, the removal effect of Cu^{2+} was determined by the adsorption quantity (q_t), which was calculated according to Eq. (1):

$$q_t = \frac{C_0 - C_t}{m} \times V \quad (1)$$

where C_0 represents the initial Cu(II) concentration in the solutions (mg L^{-1}), C_t refers to the concentration of Cu^{2+} (mg L^{-1}) at time t, m is the dosage (g) of adsorbent used, and V means the solution volume (L).

Table 1 Main chemical compositions of MSR and CMSR (wt%)

Sample	Al_2O_3	CaO	Fe_2O_3	K_2O	MgO	MnO	Na_2O	P_2O_5	SiO_2	SO_3	TiO_2	LOI
MSR	3.92	0.89	23.80	0.44	0.31	9.73	0.15	0.68	43.92	7.45	0.18	13.21
CMSR	7.42	0.03	64.90	0.01	0.02	2.91	0.01	1.90	2.66	0.01	0.09	18.78

Adsorption kinetics and isotherms

To examine the adsorption process, pseudo-first-order and pseudo-second-order (Agarwal et al. 2016; Gupta et al. 2017) kinetic models were used in this study. The two kinetic models are applied and analyzed according to Eqs. (2) and (3) (Marques et al. 2019; Zou et al. 2019), respectively, as follows:

$$q_t = q_e\left(1-e^{-k_1 t}\right) \tag{2}$$

$$q_t = \frac{t}{\left(1/k_2 q_e^2\right) + \left(t/q_e\right)} \tag{3}$$

where q_e (mg g^{-1}) refers to the amount of copper ions adsorbed at equilibrium, q_t (mg g^{-1}) is the amount of copper ions adsorbed at time t (min), and k_1 (min^{-1}) and k_2 (g mg^{-1} min^{-1}) represent the pseudo-first-order adsorption rate constant and the equilibrium rate constant of pseudo-second-order adsorption, respectively.

The experimental data in this study were analyzed based on the Langmuir and Freundlich isothermal adsorption models. The Langmuir isotherm model is usually expressed as Eq. (4) (Marques et al. 2019; Zou et al. 2019).

$$q_e = \frac{q_{max} K_L C_e}{1 + K_L C_e} \tag{4}$$

where C_e (mg L^{-1}) represents the Cu^{2+} equilibrium concentration in the system, q_e (mg g^{-1}) is the amount of adsorbate per unit mass of adsorbent at equilibrium, and q_{max} (mg g^{-1}) and K_L refer to the maximum adsorption capacity and the Langmuir constant related to the adsorption capacity, respectively.

The Freundlich isotherm model can be used to evaluate the adsorption intensity of copper ions onto the CMSR surface. The model is expressed as follows (Eq. (5)):

$$q_e = K_F C_e^{1/n_F} \tag{5}$$

where K_F ((mg g^{-1})(mg L^{-1})$^{-1/nF}$) is the Freundlich adsorption constant, and $1/n_F$ is the heterogeneity factor referring to the adsorption intensity.

Results and discussion

Characterization of CMSR

Table 1 presents the main chemical compositions of MSR and CMSR. It can be seen from the table that the main chemical constituents of MSR are SiO_2, Fe_2O_3, MnO, SO_3, and Al_2O_3, and the contents of the other elements are lower than 1 wt%. The main chemical constituents of CMSR are Fe_2O_3 and Al_2O_3. Iron oxide occurs as the main component in CMSR, and its content is as high as 64.9 wt%. The process of hydrothermal conversion effectively enriches iron and removes potassium, calcium, sodium, magnesium and especially sulfur and silicon. After the treatment, the SiO_2 and SO_3 contents decreased from 43.92 and 7.45 wt%, respectively, to 2.66 and

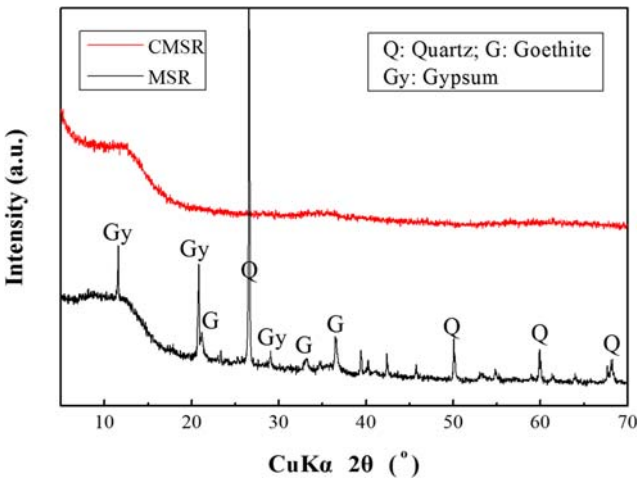

Fig. 1 XRD patterns of MSR and CMSR

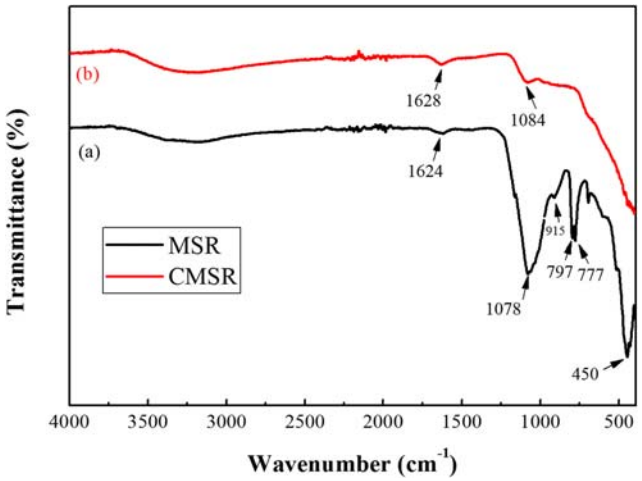

Fig. 2 FTIR spectra of MSR (a) and CMSR (b)

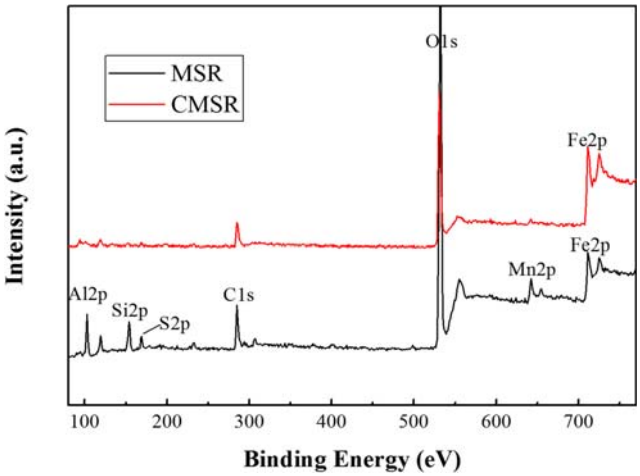

Fig. 3 XPS high-resolution spectra of MSR and CMSR

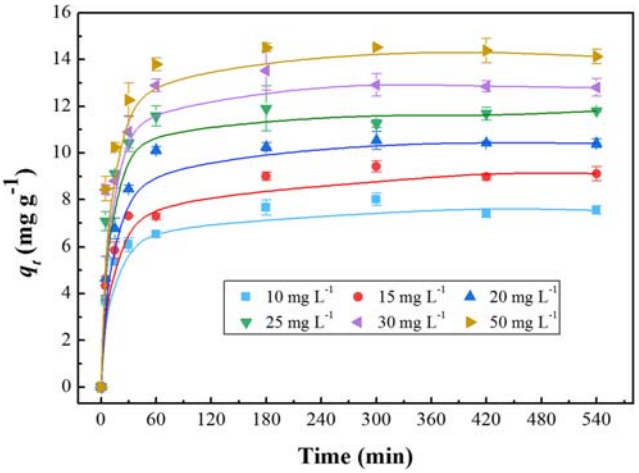

Fig. 5 Effect of the contact time on the adsorption of copper ions onto CMSR

0.01 wt%, respectively. The results indicate that an iron-rich adsorbent, CMSR, from manganese sulfate residue has been obtained.

Figure 1 compares the XRD patterns of MSR and CMSR. Combined with the main chemical constituents of MSR in Table 1, the main phase of MSR is quartz, goethite, and gypsum. No mineralogical phase containing manganese was found in the XRD pattern of MSR, which may be mainly due to the amorphous phase occurrence of manganese. As previously reported (Yang et al. 2018), there were amounts of water soluble Mn^{2+} in the similar MSR sample. The diffraction pattern of CMSR has no diffraction peaks, implying that the obtained CMSR is amorphous.

MSR and CMSR samples were analyzed by infrared spectroscopy and XPS. The results of FTIR spectra of MSR and CMSR are shown in Fig. 2a and b, respectively. As shown in Fig. 2a, MSR exhibits absorption bands at 1078, 797, 777, and 450 cm^{-1} corresponding to SiO_2 (Godočíková et al. 2002; Jeon et al. 2003; Fan et al. 2012). Specifically, the bands at 797 and 450 cm^{-1} are due to the Si–O–Si symmetric stretching and bending vibrations, respectively (Jeon et al. 2003). The series of absorption bands vanish in the FTIR spectra of CMSR (as shown in Fig. 2b), which demonstrates that the SiO_2 in CMSR is mostly removed after the hydrochloric acid treatment. Moreover, a new band appears at approximately 1084 cm^{-1} in the spectrum of CMSR (Fig. 2b), which may also be the Si–O-stretching band (Shoval et al. 2011). The H–O–H vibration band at 1624 cm^{-1}, which is ascribed to the adsorbed water, coordinated water and zeolite water in MSR, shifted to 1628 cm^{-1} in CMSR (Shu et al. 2018). The results show that the hydrothermal conversion process can effectively remove silicon.

Figure 3 shows the XPS results of MSR and CMSR. The wide-scan XPS spectrum of MSR shows diffraction peaks of C1s, O1s, Fe2p, Mn2p, Al2p, and Si2p with corresponding binding energies at 284.98, 531.16, 710.13, 640.42, 104.58, and 154.17 eV, respectively (Lan et al. 2019). However, Si2p, S2p, and Mn2p disappear in the XPS spectrum of CMSR, indicating the effective removal of these elements during the hydrothermal conversion process.

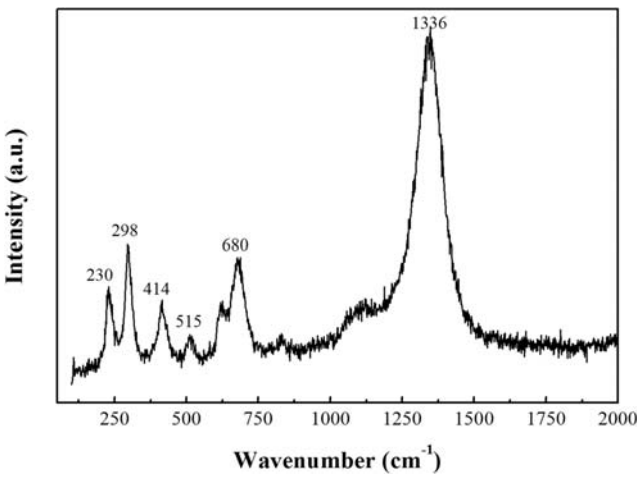

Fig. 4 Raman spectrum of CMSR

Table 2 Adsorption capacities of copper ions by other adsorbents

Absorbent	q_e (mg g^{-1})	Reference
Bentonite	7.04	Freitas et al. (2017)
Biogenic oyster shells	8.90	Wu et al. (2014)
Chitin/chitosan hydroxyapatite	5.00	Gandhi et al. (2011)
Chitosan-coated sand	8.18	Wan et al. (2010)
Fish waste	1.20	Haouti et al. (2019)
Low-temperature biochar	5.00	Hoslett et al. (2019)
Natural foxtail millet shells	11.89	Peng et al. (2018)
Porous ceramsite	9.42	Jing et al. (2018)

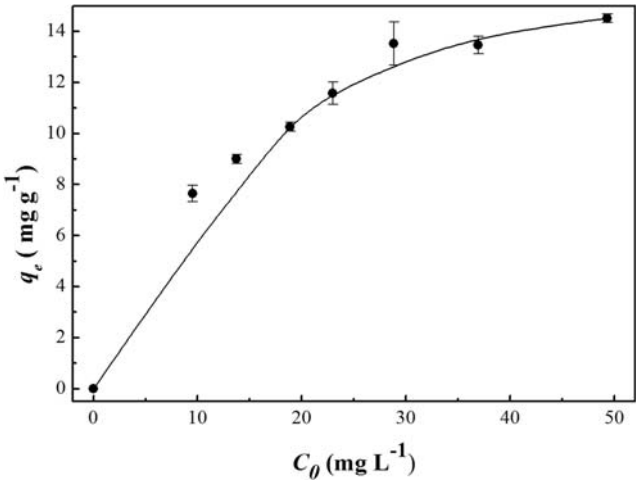

Fig. 6 Effect of the initial concentration on the adsorption of Cu^{2+} onto CMSR

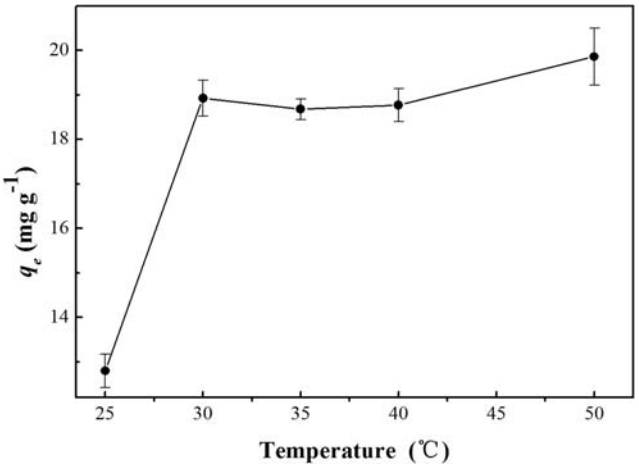

Fig. 8 Effect of the reaction temperature on the adsorption of Cu^{2+} onto CMSR

The Raman spectrum of CMSR exhibits strong and weak bands at 230, 298, 414, 515, 680, and 1336 cm^{-1}, as shown in Fig. 4. The existence of bands at 230, 298, 414, and 680 cm^{-1} was reported as α-FeOOH (Thibeau et al. 1978; Hanesch 2009). Whereas, Oh et al. (1998) considered that the band appeared at 1336 cm^{-1} could be assigned to $Fe(OH)_3$. As discussed, the XRD results suggest that no crystalline iron-containing minerals are presented in the diffraction pattern of CMSR. Therefore, it can be concluded that iron-containing components constitute the main composition of CMSR, namely, an amorphous form of FeOOH or $Fe(OH)_3$.

Effect of the contact time

In the current study, CMSR adsorption equilibrium experiments were first conducted. Figure 5 shows the effect of the contact time on the adsorption of Cu^{2+} onto CMSR at different initial Cu^{2+} concentrations. As seen from the curves, the adsorption quantity increases with time and reaches an equilibrium at 180 min. With increasing of the initial Cu^{2+} concentration to 50 mg L^{-1}, the adsorption capacity gradually increased up to 14.515 mg g^{-1}. The adsorption capacity of CMSR at 50 mg L^{-1} is higher than those of many other adsorbents for copper ions as tabulated in Table 2. For the sake of comparison, an adsorption experiment using MSR at a copper ions concentration of 10 mg L^{-1} was also carried out. At a reaction time of 180 min, the MSR adsorption capacity is only 2.110 mg g^{-1}, while the CMSR adsorption capacity reaches as high as 7.653 mg g^{-1} (Fig. 5) at the same initial Cu^{2+} concentration. Hence, the adsorption capacity of CMSR is significantly improved compared with that of the original MSR.

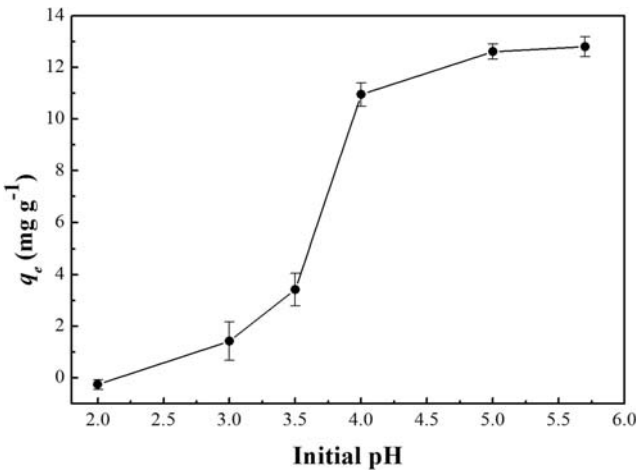

Fig. 7 Effect of the initial pH on the adsorption of Cu^{2+} onto CMSR

Effects of the initial concentration, initial pH, and temperature

The adsorption of 7 groups of copper sulfate solutions with different initial concentrations by CMSR was studied. Figure 6 shows the effect of the initial Cu^{2+} concentration on the adsorption capacity of CMSR for Cu^{2+} at room temperature and natural pH. The results show that with the increase of initial Cu^{2+} concentration, the adsorption capacity of CMSR gradually increased, and the adsorption capacity tended to stabilize. Further increasing the initial concentration will not increase the adsorption capacity significantly. It has been reported the driving force generated from initial concentration could overcome the resistance of adsorbates mass transfer (Wan et al. 2010; Shu et al. 2018). Therefore, the adsorption process depends on initial concentration of adsorbates.

Experiments referring to pH investigation were carried out at pH value less than 6.0 to ensure that the copper ions are soluble without precipitation in the solution (Wan et al. 2010). When the pH is higher than 6.0, precipitation usually occurs in the presence of copper ions. Figure 7 shows the effect of the different initial pH on the adsorption equilibrium at room temperature using the Cu^{2+} concentration of 30 mg L^{-1}. The

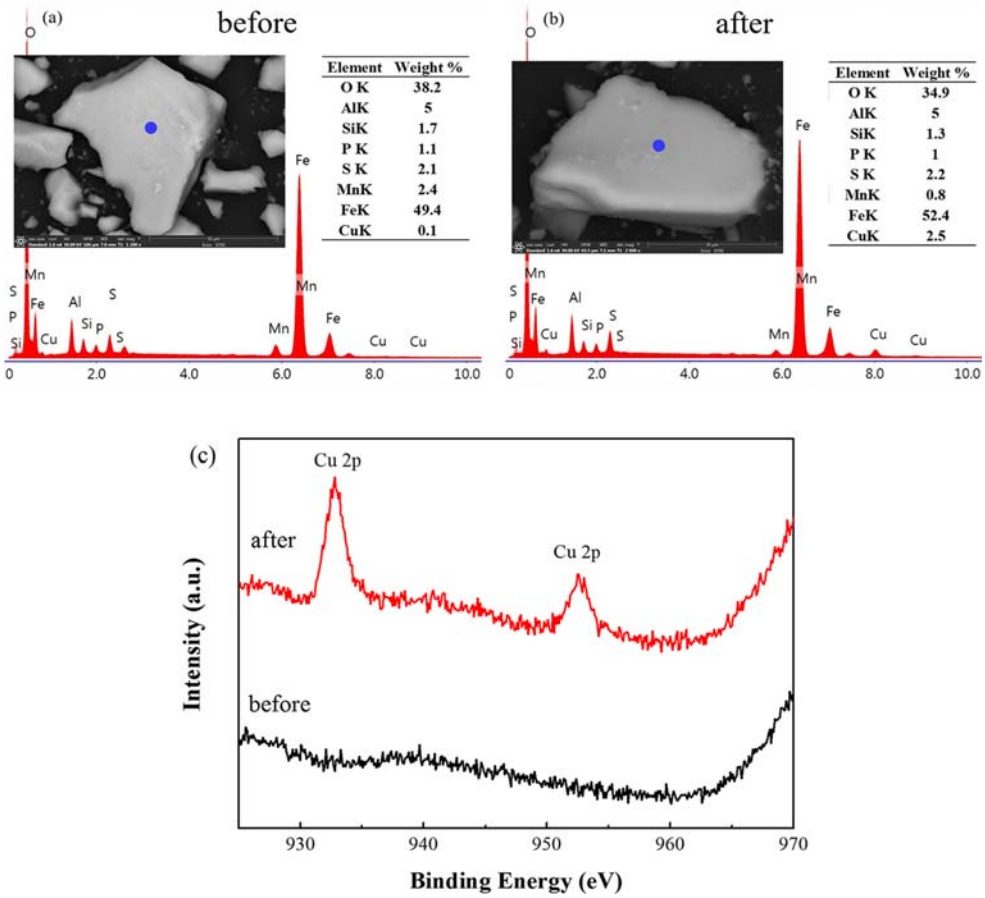

Fig. 9 EDS spectra of CMSR before (**a**) and after (**b**) Cu^{2+} adsorption; XPS high-resolution spectra of Cu2p before and after Cu^{2+} adsorption (**c**)

initial pH of the solution was adjusted with 0.05 mol L^{-1} H_2SO_4. When the pH value changed from 2.0 to 5.7 (natural pH), the adsorption capacity of CMSR increased from 0 to 12.801 mg g^{-1}. At a lower pH value, a low adsorption capacity was determined. It is certain that the hydrogen ions (H^+) concentration in the solution is higher at lower pH values. Due to this reason, the predominant H^+ can compete with Cu^{2+} in the solution (Wan et al. 2010; Jiang et al. 2015), resulting in a lower adsorption capacity of Cu^{2+}. On the contrary, a higher pH level promotes deprotonation of the adsorbent surface, which increases the number of negatively charged sites (Roy and Bhattacharya 2012; Shakoor and Nasar 2016; Haouti et al. 2019). Furthermore, the increase of negatively charged sites raises the applied forces that connect Cu^{2+} and the adsorbent surfaces, resulting in an increase in the adsorption capacity (Roy and Bhattacharya 2012).

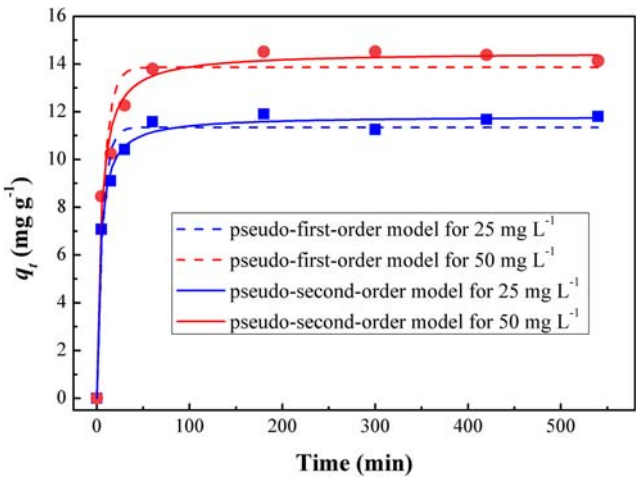

Fig. 10 Plots of the pseudo-first-order and the pseudo-second-order kinetics model for the adsorption of copper ion onto CMSR

The solution temperature is a crucial parameter to elucidate the interaction mechanism of adsorption system (Dou et al. 2019). In this study, the adsorption process at the Cu^{2+} concentration of 30 mg L^{-1} with natural pH was investigated at a series of contact temperatures in the range of 25–50 °C, and the experimental data are illustrated in Fig. 8. It is observed that the adsorption capacity increased with increasing temperature. When increasing the temperature from 25 to 30 °C, q_e of CMSR for Cu^{2+} significantly increases from 12.801 to 18.928 mg g^{-1}. The increasing temperature can accelerate the mobility and randomness of the Cu^{2+} in the solution. It can be inferred that the significant increase of adsorption capacity occurs, as well as the chemical interactions increasingly happens (Dou et al. 2019). Therefore, more copper ions can arrive at the active sites of CMSR. However, the adsorption

Table 3 Constants and correlation coefficients from the pseudo-first-order and the pseudo-second-order kinetic models for Cu^{2+} adsorption onto CMSR

	$q_{e,exp}$ (mg g^{-1})	Pseudo-first-order kinetic constant			Pseudo-second-order kinetic constant		
		$q_{e,cal}$ (mg g^{-1})	k_1 (min^{-1})	R^2	$q_{e,cal}$ (mg g^{-1})	k_2 (g mg^{-1} min^{-1})	R^2
25 mg L^{-1}	11.908	11.349	0.160	0.966	11.817	0.023	0.993
50 mg L^{-1}	14.515	13.861	0.135	0.944	14.487	0.016	0.988

capacity trend with regard to temperatures higher than 30 °C shows a slight increase. With a further increase in temperature from 30 to 50 °C, the adsorption capacity increases only 0.932 mg g^{-1}. Based on the experimental data, it can be concluded that the adsorption is an endothermic process.

SEM and XPS analysis

To identify the form of the copper ions adsorbed onto CMSR, the adsorbent before and after adsorption was subjected to SEM and XPS analysis. The EDS spectra before and after adsorption of copper ions onto CMSR are presented in Fig. 9a and b. From several points detected, the contents of Cu on original CMSR particles are 0.1 wt%. After Cu^{2+} adsorption onto CMSR, the EDS spectrum shows a Cu peak, and the copper ions on the surface occur at a content of approximately 2.5 wt%. The results also demonstrate that copper ions have been adsorbed on the surface of the CMSR adsorbent.

Figure 9 c shows the high-resolution XPS results. Cu2p peaks appear at characteristic binding energies of 932.8 eV and 952.6 eV, which are similar to those of copper ions adsorbed onto other materials (Chen et al. 2018). The 952.6 eV peak can be attributed to the reaction of the hydroxyl group with Cu^{2+} (Chen et al. 2018). This result is consistent with the analysis of the EDS spectra and further confirms that Cu^{2+} has been adsorbed on the surface of CMSR.

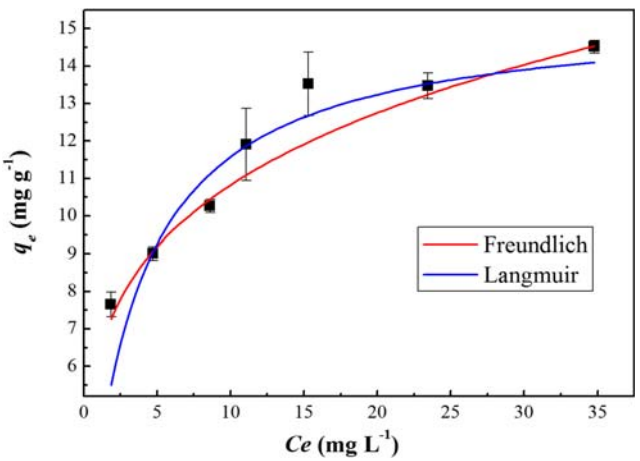

Fig. 11 Langmuir and Freundlich isotherm models for the adsorption of Cu^{2+} onto CMSR

Adsorption kinetics

Figure 10 shows the kinetic curves of the experimental data at initial copper ions concentrations of 25 and 50 mg L^{-1} onto the CMSR adsorbent, exhibiting the plots of the nonlinear form of the pseudo-first-order model and pseudo-second-order model. The adsorption rate constants calculated from the plots of kinetic models and the correlation coefficients (R^2) are listed in Table 3.

The accuracy of the fitted kinetic model value can be reflected by comparing the calculated $q_{e,cal}$ values and experimental data ($q_{e,exp}$) (Cheng et al. 2019). The values of $q_{e,cal}$ calculated from the models do not deviate from $q_{e,exp}$ at both concentrations. The $q_{e,cal}$ values of pseudo-second-order model are closer to $q_{e,exp}$ values. In addition, the correlation coefficients R^2 of the pseudo-second-order model are larger. Based on this finding, pseudo-second-order kinetic mode is suggested to be more consistent with the adsorption process of Cu(II) onto the CMSR adsorbent in this study. For heterogeneous adsorbents the majority of the metal ion adsorption kinetics follows pseudo-second-order mechanisms (Wan et al. 2010). The pseudo-second-order mode is generally interpreted that the mechanism of the adsorption process is mainly controlled by chemical bonding or chemisorptions (Guo et al. 2018). In the current work, an occurrence of chemical adsorption for the iron hydroxide adsorbent can be understood as the reaction of Cu^{2+} with the surface hydroxyl groups on CMSR.

Adsorption isotherms

Adsorption isotherms can represent the relationship between q_e and C_e in the adsorption system. Langmuir and Freundlich isothermal adsorption models are frequently employed to designate the adsorption equilibrium. The Langmuir isotherm refers to the formation of a single layer of homogeneous adsorption on the surface of the adsorbent, whereas the Freundlich adsorption isotherm describes a heterogeneous surface due to the adsorption capacity and adsorption intensity with irregular multilayer adsorption (Agarwal et al. 2016; Cheng et al. 2019).

Figure 11 shows the Langmuir and Freundlich adsorption isotherms, respectively. The values of relevant parameters

Table 4 Constants of adsorption isotherm for Cu^{2+} adsorption onto CMSR

Isotherm	Parameters		R^2
Langmuir	$q_{max} = 15.454$ mg g^{-1}	$K_L = 0.299$ L mg^{-1}	0.877
Freundlich	$K_F = 6.281$ (mg g^{-1})(mg $L^{-1})^{-1/nF}$	$1/n_F = 0.236$	0.988

were calculated from the plots and the results are tabulated in Table 4. The maximum uptake capacity (q_{max}) for copper ions onto the CMSR adsorbent was calculated to be 15.454 mg g^{-1} from the Langmuir model. The numerical value of Freundlich constants $1/n_F < 1$ indicates that the adsorption is a favorable process (Wan et al. 2010; Kan et al. 2015; Nayak and Pal 2017). The correlation coefficient R^2 when considering the Langmuir isotherm model is 0.877, which is higher than that when considering the Freundlich isotherm model (0.988). However, the parameters of different forms of the Langmuir isotherm are different (Parimal et al. 2010). The nonlinear form of Langmuir equation used in this study has lower correlation coefficients. Clearly, the fit of the Freundlich isotherm to the experimental data is better than that of the Langmuir isotherm to the experimental data. From the R^2 obtained from nonlinear estimation in this study, it suggests that the adsorption of Cu^{2+} onto CMSR is well fitted with the Freundlich isotherm model. Since the Freundlich model is an empirical equation to describe heterogeneous systems, it can be concluded that the surface hydroxyl groups on CMSR that reacted with adsorbate have diverse sources. For most adsorption research work, desorption and reuse of adsorbents are performed by chemical means (Marques et al. 2019). In the case of CMSR in this work, desorption is not involved since the iron-containing adsorbent from industrial waste and the material has a low cost.

Conclusions

Manganese sulfate residue (MSR) is a high iron-containing industrial waste discharged from the sulfuric acid leaching process of manganese-bearing ores. An amorphous iron hydroxide adsorbent (CMSR) was prepared from MSR. The present research proves that CMSR is a good adsorbent to remove copper ion in solution. CMSR has an adsorption capacity of 7.653 mg g^{-1} for initial Cu^{2+} concentration at 10 mg L^{-1}, much higher than that of MSR (2.110 mg g^{-1}). The equilibrium adsorption capacity of the adsorbent for initial Cu^{2+} concentration at 50 mg L^{-1} was as high as 14.515 mg g^{-1}. The adsorption process can be influenced by several factors, such as the contact time, initial copper ions concentration, initial pH value, and reaction temperature. The experimental results are in accordance with the pseudo-second-order kinetic, indicating that the adsorption behavior is most likely chemical adsorption. The adsorption behavior is consistent with the Freundlich isothermal adsorption model. In this study, the CMSR adsorption prepared from MSR is able to remove copper ions from the aqueous solutions. Taken together, MSR has the potential to become a raw material for preparing adsorbent in environmental applications.

Acknowledgments The work was financially supported by the National Natural Science Foundation of China (Grant No. U1812402; 41972048), National Key Research and Development Program of China (2018YFC1903500), and Guizhou Provincial Science and Technology Foundation (No. [2016]1155). The authors are grateful to Mr. S. Yang for FTIR determination.

References

Agarwal S, Sadegh H, Monajjemi M, Hamdy AS, Ali GAM, Memar AOH, Shahryari-ghoshekandi R, Tyagi I, Gupta VK (2016) Efficient removal of toxic bromothymol blue and methylene blue from wastewater by polyvinyl alcohol. J Mol Liq 218:191–197

Chen D, Liu X, Nie H (2018) Crumpled graphene balls as rapid and efficient adsorbents for removal of copper ions. J Colloid Interf Sci 530:46–51

Cheng H, Zhu Q, Xing Z (2019) Adsorption of ammonia nitrogen in low temperature domestic wastewater by modification bentonite. J Clean Prod 233:720–730

Dou J, Huang Q, Huang H, Gan D, Chen J, Deng F, Wen Y, Zhu X, Zhang X, Wei Y (2019) Mussel-inspired preparation of layered double hydroxides based polymer composites for removal of copper ions. J Colloid Interf Sci 533:416–427

Fan F, Qin Z, Bai J, Rong W, Fan F, Tian W, Wu X, Wang Y, Zhao L (2012) Rapid removal of uranium from aqueous solutions using magnetic Fe_3O_4@SiO_2 composite particles. J Environ Radioactiv 106:40–46

Freitas ED, Carmo ACR, Almeida Neto AF, Vieira MGA (2017) Binary adsorption of silver and copper on Verde-lodo bentonite: kinetic and equilibrium study. Appl Clay Sci 137:69–76

Gandhi MR, Kousalya GN, Meenakshi S (2011) Removal of copper (II) using chitin/chitosan nano hydroxyapatite composite. Int J Biol Macromol 48:119–124

Garba ZN, Bello I, Galadima A, Lawal AY (2016) Optimization of adsorption conditions using central composite design for the removal of copper (II) and lead (II) by defatted papaya seed. Karbala Int J Mod Sci 2:20–28

Godočíková E, Baláž P, Bastl Z, Brabec L (2002) Spectroscopic study of the surface oxidation of mechanically activated sulphides. Appl Surf Sci 200:36–47

Guo T, Yang H, Liu Q, Gu H, Wang N, Yu W, Dai Y (2018) Adsorptive removal of phosphate from aqueous solutions using different types of red mud. Water Sci Technol 2017(2):570–577

Gupta VK, Agarwal S, Bharti AK, Sadegh H (2017) Adsorption mechanism of functionalized multi-walled carbon nanotubes for advanced Cu (II) removal. J Mol Liq 230:667–673

Hanesch M (2009) Raman spectroscopy of iron oxides and (oxy) hydroxides at low laser power and possible application in environmental magnetic studies. Geophys J Int 177:941–948

Haouti REL, Anfar Z, Chennah A, Amaterz E, Zbair M, Alem NEL, Benlhachemi A, Ezahri M (2019) Synthesis of sustainable mesoporous treated fish waste as adsorbent for copper removal. Groundw Sustain Dev 8:1–9

Hoslett J, Ghazal H, Ahmad D, Jouhara H (2019) Removal of copper ions from aqueous solution using low temperature biochar derived from the pyrolysis of municipal solid waste. Sci Total Environ 673:777–789

Hosseinzadeh H, Pashaei S, Hosseinzadeh S, Khodaparast Z, Ramin S, Saadat Y (2018) Preparation of novel multi-walled carbon nanotubes nanocomposite adsorbent via RAFT technique for the adsorption of toxic copper ions. Sci Total Environ 640-641:303–314

Jeon HJ, Yi SC, Oh SG (2003) Preparation and antibacterial effects of Ag–SiO_2 thin films by sol–gel method. Biomaterials 24:4921–4928

Jiang T, Liu W, Mao Y, Zhang L, Cheng J, Gong M, Zhao H, Dai L, Zhang S, Zhao Q (2015) Adsorption behavior of copper ions from aqueous solution onto graphene oxide–CdS composite. Chem Eng J 259:603–610

Jing Q, Wang Y, Chai L, Tang C, Huang X, Guo H, Wang W, You W (2018) Adsorption of copper ions on porous ceramsite prepared by diatomite and tungsten residue. T Nonferr Metal Soc 28(5):1053–1060

Kan S, Sun B, Xu F, Song Q, Zhang S (2015) Biosorption of aquatic copper (II) by mushroom biomass Pleurotus eryngii: kinetic and isotherm studies. Water Sci Technol 71(2):283–288

Lan J, Sun Y, Guo L, Li Z, Du D, Zhang T (2019) A novel method to recover ammonia, manganese and sulfate from electrolytic manganese residues by bio-leaching. J Clean Prod 223:49–507

Marques BS, Frantz TS, Sant'Anna Cadaval Junior TR, de Almeida Pinto LA, Dotto GL (2019) Adsorption of a textile dye onto piaçava fibers: kinetic, equilibrium, thermodynamics, and application in simulated effluents. Environ Sci Pollut Res 26:28584–28592

Mezenner NY, Bensmaili A (2009) Kinetics and thermodynamic study of phosphate adsorption on iron hydroxide-eggshell waste. Chem Eng J 147:87–96

Nadaroglu H, Kalkan E, Demir N (2010) Removal of copper from aqueous solution using red mud. Desalination 251:90–95

Nayak AK, Pal A (2017) Green and efficient biosorptive removal of methylene blue by abelmoschus esculentus seed: process optimization and multi-variate modeling. J Environ Manag 200:145–159

Oh SJ, Cook DC, Townsend HE (1998) Characterization of iron-oxides commonly formed as corrosion products on steel. Hyperfine Interact 112:59–65

Parimal S, Prasad M, Bhaskar U (2010) Prediction of equillibrium sorption isotherm: comparison of linear and nonlinear methods. Ind Eng Chem Res 49(6):2882–2888

Peng S, Wang R, Yang L, He L, He X, Liu X (2018) Biosorption of copper, zinc, cadmium and chromium ions from aqueous solution by natural foxtail millet shell. Ecotox Environ Safe 16:61–69

Pengsaket I, Thamaphat K, Limsuwan P (2016) Removal of Cu (II) from aqueous solutions by magnetic nanoparticles-pomelo peel composite. Key Eng Mater 675-676:154–157

Roy A, Bhattacharya J (2012) Removal of Cu (II), Zn (II) and Pb (II) from water using microwave-assisted synthesized maghemite nanotubes. Chem Eng J 211-212:493–500

Shakoor S, Nasar A (2016) Removal of methylene blue dye from artificially contaminated water using Citrus limetta peel waste as a very low cost adsorbent. J Taiwan Inst Chem E 66:154–163

Shoval S, Yadin E, Panczer G (2011) Analysis of thermal phases in calcareous Iron Age pottery using FT-IR and Raman spectroscopy. J Therm Anal Calorim 104:515–525

Shu J, Liu R, Liu Z, Du J, Tao C (2016) Manganese recovery and ammonia nitrogen removal from simulation wastewater by pulse electrolysis. Sep Purif Technol 168:107–113

Shu J, Liu R, Wu H, Liu Z, Sun X, Tao C (2018) Adsorption of methylene blue on modified electrolytic manganese residue: kinetics, isotherm, thermodynamics and mechanism analysis. J Taiwan Inst Chem E 82:351–359

Shu J, Wu H, Chen M, Peng H, Li B, Liu RL, Liu Z, Wang B, Huang T, Hu Z (2019a) Fractional removal of manganese and ammonia nitrogen from electrolytic metal manganese residue leachate using carbonate and struvite precipitation. Water Res 153:229–238

Shu J, Wu H, Chen M, Wei L, Wang B, Li B, Liu R, Liu Z (2019b) Simultaneous optimizing removal of manganese and ammonia nitrogen from electrolytic metal manganese residue leachate using chemical equilibrium model. Ecotox Environ Safe 172:273–280

Song Y, Kong A, Ji Y, He B, Wang H, Li J (2019) Adsorption for copper (II) ion with chitosan-SP/PET composite adsorbent enhanced by electric field. Adsorpt Sci Technol 37(3–4):274–287

Thibeau RJ, Brown CW, Heidersbach RH (1978) Raman spectra of possible corrosion products of iron. Appl Spectrosc 32:532–535

Visa M (2016) Synthesis and characterization of new zeolite materials obtained from fly ash for heavy metals removal in advanced wastewater treatment. Powder Technol 294:338–347

Wan M, Kan C, Rogel BD, Dalida MLP (2010) Adsorption of copper (II) and lead (II) ions from aqueous solution on chitosan coated sand. Carbohyd Polym 80:891–899

Wang J, Zhang L, Zhang T, Du T, Li T, Yue T, Li Z, Wang J (2019) Selective removal of heavy metal ions in aqueous solutions by sulfide-selector intercalated layered double hydroxide adsorbent. J Mater Sci Technol 35:1809–1816

Wu Q, Chen J, Clark M, Yu Y (2014) Adsorption of copper to different biogenic oyster shell structures. Appl Surf Sci 311:264–272

Xie X, Deng R, Pang Y, Bai Y, Zheng W, Zhou Y (2017) Adsorption of copper (II) by sulfur microparticles. Chem Eng J 314:434–442

Yang Y, Gu H, Guo T, Dai Y, Wang N (2018) Environmental assessment of manganese sulfate residues derived from pyrolusite process. Fresenius Environ Bull 27(7):4883–4888

Zou C, Jiang W, Liang J, Sun X, Guan Y (2019) Removal of Pb(II) from aqueous solutions by adsorption on magnetic bentonite. Environ Sci Pollut Res 26:1315–1322